NUCL SCI TECH (2017) 28:172
https://doi.org/10.1007/s41365-017-0324-6

Precise magnetic field control of the scanning magnets for the APTRON beam delivery system

Chun-Hui Miao[1,2] · Ming Liu[1] · Chong-Xian Yin[1] · Zhen-Tang Zhao[1]

Received: 20 June 2017 / Revised: 21 August 2017 / Accepted: 7 September 2017 / Published online: 16 November 2017

Abstract A design for precise scanning magnetic field control for the beam delivery system of the Shanghai Advanced Proton Therapy Facility (APTRON) is presented in this paper. With a novel feedforward algorithm to compensate for magnet hysteresis, the scanning magnetic field can be controlled to within a precision of $\pm$ 2.5 G. The main advantage of the proposed feedforward algorithm is that the average settling time is shorter compared with that of a conventional feedback algorithm with acceptable tolerance.

Keywords Proton therapy · Scanning magnet · Hysteresis · Feedforward control

1 Introduction

Proton beams have been widely used in cancer therapy for the past few decades. The Shanghai Advanced Proton Therapy Facility (APTRON) is the first Chinese-developed, hospital-based proton therapy facility, and it is under construction at the time of writing [1].

The beam delivery system is one of the key systems in a proton therapy facility. Its function is to achieve the prescribed dose rate and three-dimensional dose distribution. Beam delivery systems commonly use a spot-scanning technique, which is also implemented in the APTRON beam delivery system. The distinct advantages of a spot-scanning beam delivery system are its lack of patient-specific hardware, precise three-dimensional conformal dose distribution, and excellent distal dose fall-off performance.

2 The APTRON beam delivery system

A schematic diagram of the spot-scanning beam delivery system is shown in Fig. 1. Two orthogonal scanning magnets (SMU and SMV) are used to control the irradiation position of the proton beam. A photo of the SMU scanning magnet is shown in Fig. 2. The main design parameters of the scanning magnets are presented in Table 1.

The workflow of the spot-scanning beam delivery system during the irradiation process is as follows:

(1) The beam is moved to the prescribed position.
(2) The proton beam is turned on.
(3) The proton beam is turned off when the prescribed particle number has been reached.
(4) The beam is moved to the next position.

The transition time for moving the beam is part of the overall irradiation time. Therefore, the transition time should be as short as possible to achieve a high dose rate. In order to realize a high-accuracy three-dimensional dose distribution, the maximum error in the iso-center of the beam position should be within $\pm$ 0.07 mm, and the

This work was supported by the Youth Innovation Promotion Association CAS (No. 2016238).

✉ Zhen-Tang Zhao
zhaozhentang@sinap.ac.cn

1 Shanghai Institute of Applied Physics, Chinese Academy of Sciences, Shanghai 201800, China

2 University of Chinese Academy of Sciences, Beijing 100049, China

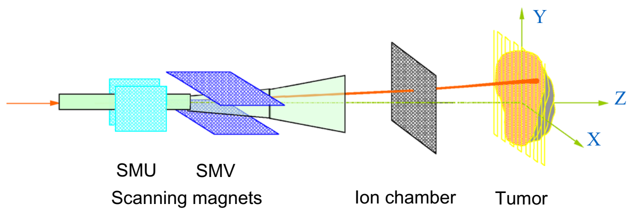

Fig. 1 (Color online) Schematic of the spot-scanning beam delivery system

Fig. 2 (Color online) SMU scanning magnet

Table 1 Specifications of the scanning magnets

Parameters	SMU	SMV
Deflection angle (mrad)	± 69.7	± 62.0
SAD (m)	2.87	2.42
Pole length (m)	0.205	0.230
Magnet length (m)	0.309	0.334
Magnet gap (mm)	30	109
Number of coil turns	48	64
Maximum field strength (T)	0.799	0.634

corresponding maximum error in the magnetic field strength should be within ± 2.5 G.

3 Hysteresis effect of the scanning magnets

Magnetic hysteresis is the main factor that influences the accuracy of the scanning magnetic field. Hysteresis can be divided into rate-dependent hysteresis and rate-independent hysteresis. Rate-dependent hysteresis involves a dynamic response to changes in the magnetic field.

Figure 3 shows the step response of the scanning magnet. When the input current of the scanning magnet changed by 5% of the maximum, the settling time of the magnetic field was less than 2 ms.

The magnetic hysteresis loop is shown in Fig. 4, which illustrates the properties of rate-independent hysteresis. Following an investigation of ferromagnetic hysteresis loops, Kuhnen summarized the following rules for rate-independent hysteresis [2]:

- Any curve C_1 emanating from a turning point A of the output–input trajectory is uniquely determined by the coordinate of A.
- If any point B on the curve C_1 becomes a new turning point, then the curve C_2 originating at B leads back to the point A.
- If the curve C_2 continues beyond the point A, then it coincides with the continuation of the curve C that led to the point A before the C_1–C_2 cycle was traversed.

Typical feedforward control strategies are a neural network control [3–5], Prandtl–Ishlinskii (PI) control [6], and generalized PI (GPI) control [7–11]. However, PI and GPI control are too complex to be realized in real-time calculation, which is necessary for control of the scanning magnetic field in the spot-scanning beam delivery system.

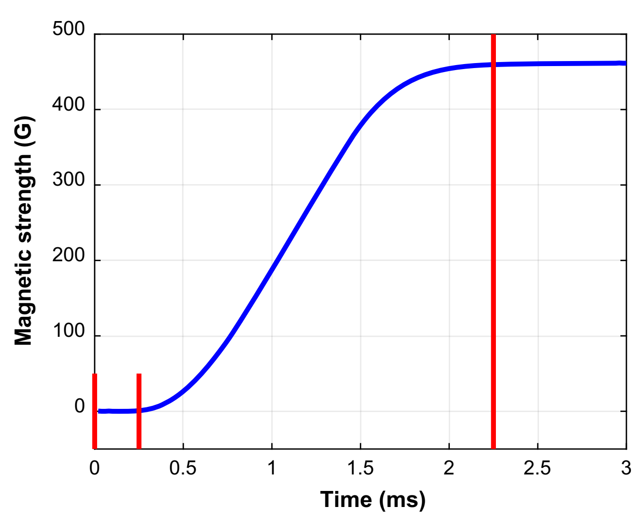

Fig. 3 (Color online) Step response of the scanning magnetic field

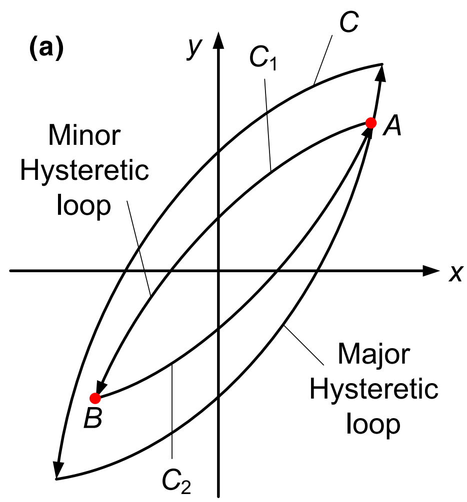

Fig. 4 Ferromagnetic hysteresis loops [2]

4 Feedforward control of the scanning magnets

For a conventional feedback system, the magnet hysteresis is compensated for by the feedback loop. However, for a feedforward system, the magnetic hysteresis should be precisely modeled in order to achieve the required accuracy for the magnetic field strength. Another consideration in developing the hysteresis model is that the model calculation should be as simple as possible to meet the needs of real-time control.

4.1 A simplified model for rate-independent hysteresis

According to Madelung's rules, any curve emanating from a turning point is uniquely determined by the coordinates of the turning point. As shown in Fig. 5, a bundle of curves may be recorded. The turning point is defined as the top point of the hysteresis loops (at the point of the arrow). The path (curve C_2 or C_5) from a starting point (the blue triangle) to a set point (the green square) is uniquely determined by the starting point.

Because hysteresis loops are multi-valued functions, the curves for the increasing current and for the decreasing current are different and are recorded separately (as shown in Fig. 5a, b).

4.2 Feedforward control algorithm

The proposed feedforward control algorithm is based on the above simplified hysteresis model.

Suppose that the initial values of the current magnetic field strength and the excitation current are B_{ini} and I_{ini}, respectively, the corresponding hysteresis curve is C, and the target magnetic field strength is B_{set}, related like so:

$$C : B = f(I).$$

The set value of the excitation current I_{set} is uniquely determined by the target magnetic field strength B_{set} and can be calculated by solving the following equation:

$$B_{\text{set}} = f(I_{\text{set}}).$$

Only a limited number of curves were recorded for the sake of practicality. If the starting point (I_{ini}, B_{ini}) was not on any of these curves, then the closest curve was selected. All curves were fitted by piecewise functions, and a linear interpolation method was implemented.

To ensure a monotonic relationship between the excitation current and the magnetic field strength, overshoot of the scanning magnet's power supply was avoided.

In order to cover the entire region of possible starting points and to ensure the accuracy of the magnetic field strength, the excitation current at the ends of all the curves was set to the maximum current $\pm I_{\max}$, and the distance between two adjacent curves at any given excitation

Fig. 5 Schematic diagrams of the feedforward control algorithm

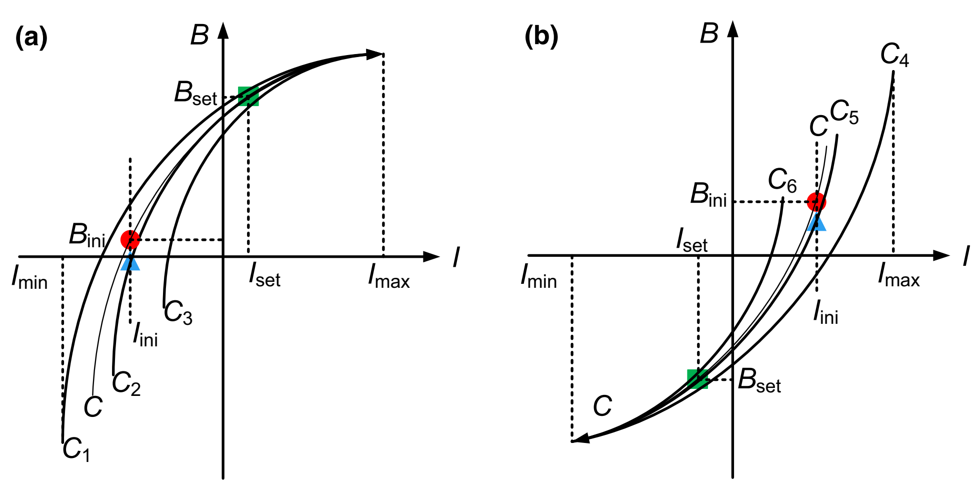

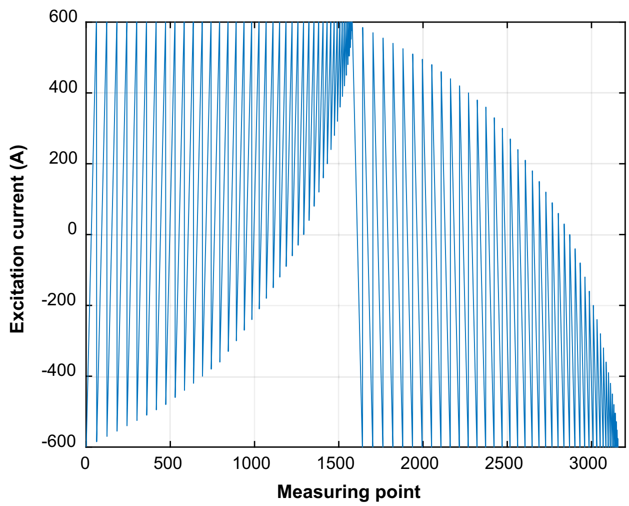

Fig. 6 (Color online) Input excitation current

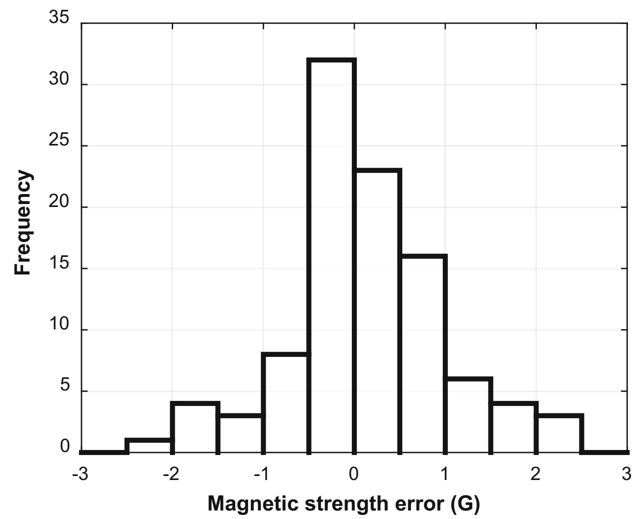

Fig. 8 Histogram of magnet strength error (feedforward)

current was within ± 2.5 G. The input current shown in Fig. 6 is:

$$I = \begin{cases} I_{\mathrm{ini}} + \Delta I \cdot i & \text{(ascending curve)} \\ I_{\mathrm{ini}} - \Delta I \cdot i & \text{(decending curve)} \end{cases},$$

where I_{ini} is the initial excitation current, ΔI is the step-size of the change in current, and i is the sequence number of each measurement point. The hysteresis curves with the linear part subtracted are illustrated in Fig. 7.

5 Experimental results

The feedforward algorithm was tested using a benchmark of 100 random setting points for the magnetic field strength, ranging between $-B_{\max}$ and $+B_{\max}$. The testing result is shown in Fig. 8. The maximum error and the mean squared error were 2.45 and 0.60 G, respectively. The major source of control error was the distance between the adjacent recorded curves, the measurement accuracy of the magnetic field strength, and the reproducibility and stability of the scanning magnet's power supply.

The accuracy of the scanning magnetic field for the conventional feedback algorithm [3] is shown in Fig. 9. Among the 100 random setting points, 79 points need two iterations, 18 points need three iterations, and 3 points need four iterations. The accuracy of the feedback algorithm is considerably better than that of the feedforward algorithm; however, if the number of iterations is larger than two, the settling time of the scanning magnetic field is too large and the prescribed dose rate cannot be achieved.

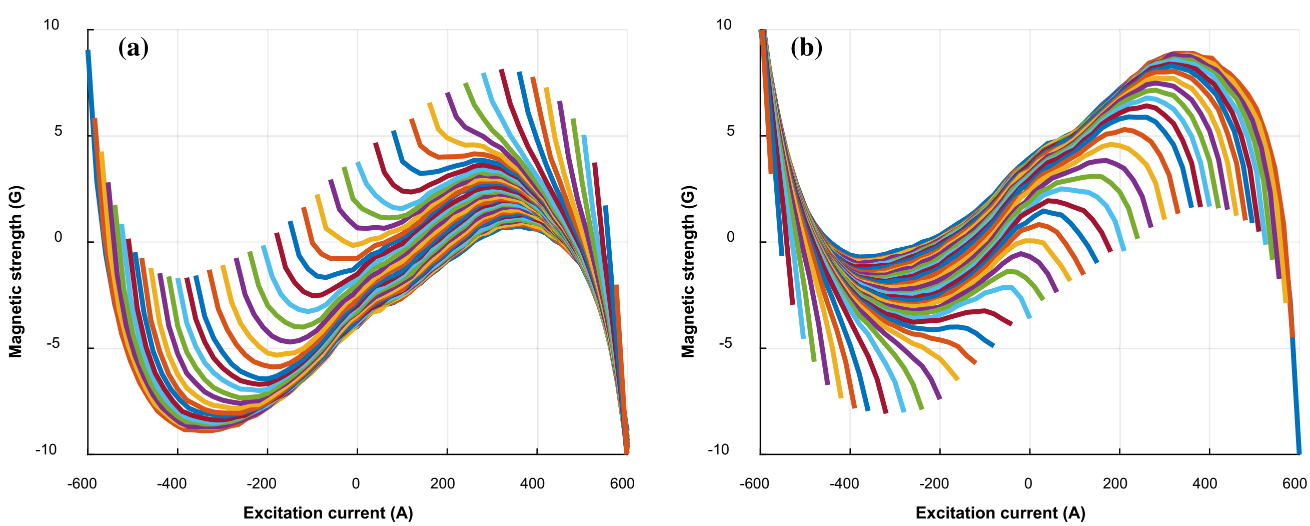

Fig. 7 (Color online) Bundles of hysteresis curves

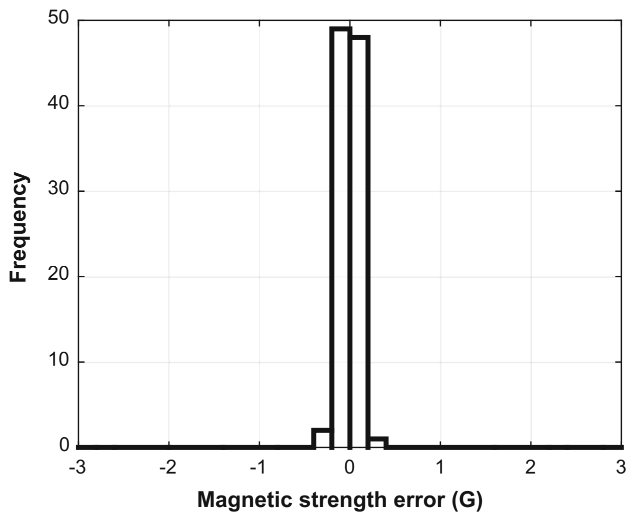

Fig. 9 Histogram of magnet strength error (feedback)

6 Discussion

From the comparison of the results of the feedforward and feedback control algorithms, we can see that the desired control precision of the magnetic field strength can be achieved through both algorithms. However, the average settling time of the proposed feedforward control algorithms is 2.2 times shorter than that of the conventional feedback algorithm. Because both algorithms can otherwise satisfy the control precision, the feedforward algorithm is preferred.

7 Conclusion

This paper proposed a novel feedforward control algorithm to achieve precise magnetic field control of the scanning magnets for the spot-scanning beam delivery system in the APTRON. The proposed feedforward algorithm was found to have better performance than the conventional feedback algorithm, owing to its shorter settling time while achieving an identical control precision of $\pm$ 2.5 G. In conclusion, the feedforward hysteresis control system meets the design requirements.

Acknowledgements We would like to thank Dr. Rui Li and Dr. Qing-Song Tan of the power supply group, and, Dr. Lian-Hua Ou-Yang and Dr. Bo-Lei Jia of the magnet group for their support.

References

1. J. Wu, H. Du, S. Xue et al., Gantry optimization of the Shanghai Advanced Proton Therapy facility. Nucl. Sci. Tech. **26**, 040201 (2015). https://doi.org/10.13538/j.1001-8042/nst.26.040201
2. K. Kuhnen, H. Janocha, Inverse feedforward controller for complex hysteretic nonlinearities in smart-material systems. Control Intell. Syst. **3**, 74–83 (2001)
3. T. Iwata, U.S. Patent 8592778, Particle beam irradiation apparatus and particle beam therapy system (2013)
4. F. Sixdenier, R. Scorretti, R. Marion et al., Quasistatic hysteresis modeling with feed-forward neural networks: influence of the last but one extreme values. J. Magn. Magn. Mater. **320**, e992–e996 (2008). https://doi.org/10.1016/j.jmmm.2008.04.076
5. C. Li, Y. Tan, A neural networks model for hysteresis nonlinearity. Sens. Actuators A Phys. **112**, 49–54 (2004). https://doi.org/10.1016/j.sna.2003.11.016
6. M. Al Janaideh, M. Rkaheja, C. Su, Compensation of hysteresis nonlinearities in smart actuators, in *ASME 2008 Conference on Smart Materials, Adaptive Structures and Intelligent Systems*, pp. 379–386 (2008). https://doi.org/10.1115/SMASIS2008-486
7. F. Stefanski, B. Minorowicz, J. Persson et al., Non-linear control of a hydraulic piezo-valve using a generalised Prandtl–Ishlinskii hysteresis model. Mech. Syst. Signal Process. **82**, 412–431 (2016). https://doi.org/10.1016/j.ymssp.2016.05.032
8. B. Minorowicz, F. Stefanski, D. Sedziak, Hysteresis modeling and position control of actuator with magnetic shape memory alloy, in *Carpathian Control Conference*, pp. 505–510 (2016). https://doi.org/10.1109/CarpathianCC.2016.7501150
9. G. Shan, Y. Li, Y. Zhang et al., Experimental characterization, modeling and compensation of rate-independent hysteresis of voice coil motors. Sens. Actuators A Phys. **251**, 10–19 (2016). https://doi.org/10.1016/j.sna.2016.09.030
10. B. Minorowicz, G. Leonetti, F. Stefanski et al., Design, modelling and control of a micro-positioning actuator based on magnetic shape memory alloys. Smart Mater. Struct. **25**, 075005 (2016). https://doi.org/10.1088/0964-1726/25/7/075005
11. J. Zhang, E. Merced, N. Sepúlveda et al., Modeling and inverse compensation of hysteresis in vanadium dioxide using an extended generalized Prandtl–Ishlinskii model. Smart Mater. Struct. **23**, 125017 (2014). https://doi.org/10.1088/0964-1726/23/12/125017